PaTS-Wheel: A Passively-Transformable Single-part Wheel for Mobile Robot Navigation on Unstructured Terrain

Thomas Godden, Barry W. Mulvey, Ellen Redgrave, and Thrishantha Nanayakkara

***Abstract*—Most mobile robots use wheels that perform well on even and structured ground, like in factories and warehouses. However, they face challenges traversing unstructured terrain such as stepped obstacles. This paper presents the design and testing of the PaTS-Wheel: a Passively-Transformable Single-part Wheel that can transform to render hooks when presented with obstacles. The passive rendering of this useful morphological feature is guided purely by the geometry of the obstacle. The energy consumption and vibrational profile of the PaTS-Wheel on flat ground is comparable to a standard wheel of the same size. In addition, our novel wheel design was tested traversing different terrains with stepped obstacles of incremental heights. The PaTS-Wheel achieved $100\ \%$ success rate at traversing stepped obstacles with heights $\approx 70\ \%$ its diameter, higher than the results obtained for an equivalent wheel ($\approx 25\ \%$ its diameter) and an equivalent wheg ($\approx 61\ \%$ its diameter). This achieves the design objectives of combining the energy efficiency and ride smoothness of wheels with the obstacle traversal capabilities of legged robots, all without requiring any sensors, actuators, or controllers.**

***Index Terms*—Compliant joints and mechanisms, embodied intelligence, underactuated robots.**

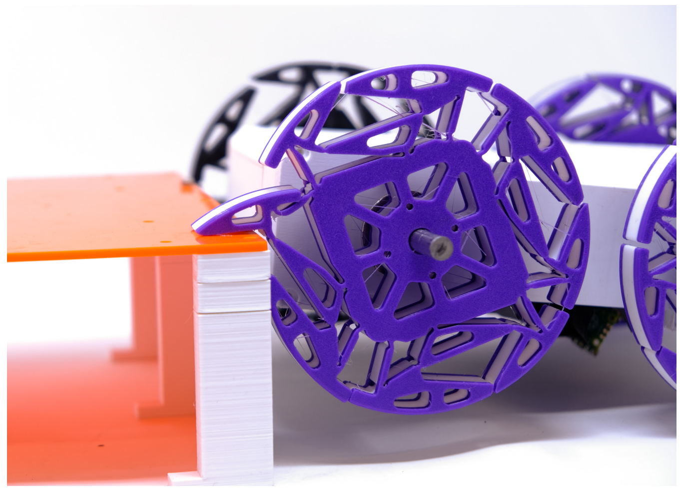

Fig. 1. The transformable PaTS-Wheel wheel traversing an obstacle. The design incorporates a flexure-based linkage which passively transforms when in contact with an object, allowing it to hook itself on and pull the robot upwards.

I. Introduction

THERE continues to be growing demand for mobile robots to emerge from structured environments—such as laboratories, factories, and warehouses—to operate in more diverse and uncalibrated surroundings. A wealth of opportunities exist in terms of applications such as inspection, maintenance, and delivery. For these implementations to become more widespread, traversal of mobile robots must be reliable such that tasks can be completed without human support or rescue.

While standard circular wheels offer ride smoothness and efficiency on uniform and structured ground, they can struggle to move over uneven terrain and obstacles which require traversal. Because of this, solutions that implement legs have been created to aid robots in overcoming more diverse landscapes.

Wheel-legs (whegs) have been a popular research choice for robots entering highly unstructured environments due to their simplified structure and control compared to full legged systems [1], [2]. However, their application has been generally limited to harsher environments; an example is the RHex robot introduced in [3] and developed by Boston Dynamics (Waltham, MA, USA). For many industrial and urban settings, the ground profiles are mostly flat except for potential curbs, stairs, or bumps that are usually known standard sizes. Current commercial applications of mobile robots in these settings carry payloads—such as inspection sensor suites, manipulators, or deliveries—which may not be suitable for prolonged vibrational movement which results from driving on whegs. Whegs also require higher torque than wheels on flat ground, reducing mission time and putting unnecessary strain on actuators, drive circuitry, and battery systems.

In previous work we developed DeforMoBot [4], a deformable mobile robot capable of using proprioceptive whisker feedback to adjust its shape in real time in order to traverse obstacles in its path. We employed a hybrid solution of different wheel types to combine the benefits of each: motor-driven rimless wheels provided traction and grip on unstructured

Manuscript received 19 December 2023; accepted 29 March 2024. This paper was recommended for publication by Editor C. Gosselin upon evaluation of the Associate Editor and Reviewers' comments. This work was supported in part by the Natural Intelligence for Robotic Monitoring of Habitats through EU Horizon 2020 Research and Innovation Programme under Grant 101016970 and in part by U.K. Engineering and Physical Sciences Research Council (EPSRC) DTP Scholarship jointly with Analog Devices, Inc. *(Thomas Godden and Barry W. Mulvey are co-first authors.) (Corresponding authors: Thomas Godden; Barry W. Mulvey.)*

The authors are with the Dyson School of Design Engineering, Imperial College London, SW7 2DB London, U.K. (e-mail: thomas.godden19@imperial.ac.uk; b.mulvey21@imperial.ac.uk; ellen.redgrave19@imperial.ac.uk; t.nanayakkara@imperial.ac.uk).

This paper has supplementary downloadable material available at https://doi.org/10.1109/LRA.2024.3389828, provided by the authors.

Digital Object Identifier (DOI): 10.1109/LRA.2024.3389828.

terrain, while passive omnidirectional wheels assisted with the robot's shape changing ability.

The aforementioned reasons have motivated the development of "transformable" wheels, which generally can switch between a wheel-like mode and a wheg-like mode based on the ground conditions. Several active versions of these mechanisms exist, but rely on additional actuators, good perception systems, and complex mechanical linkages.

In this work, we present an alternative solution—which focuses on mechanical simplicity to achieve embodied intelligence—named the PaTS-Wheel, a Passively-Transformable Single-part Wheel. Our wheel design uses a flexure-based linkage to transform when in the presence of an obstacle, allowing it to hook itself onto an object and pull itself upwards, as shown in Fig. 1. In addition to passively transforming based on terrain profile, the wheel can be printed or moulded as a single part. This increases its robustness and reduces manufacturing cost and time. The design of this wheel can be easily scaled to a desired size, meaning it can be retrofitted onto existing robots and allow them to traverse more challenging obstacles and terrain. These advantages could enhance the functionality of robots across various applications, especially those in unstructured, cluttered, or otherwise challenging environments.

The remainder of the paper is organized as follows. Section II explores relevant related work. Section III presents the methodology, including the design and kinematics of the linkage, flexure, wheel, and test robot. Section IV discusses the experiments and results of the driving power efficiency, vibrational profile, maximum climbing height, and step traversal energy consumption. The work is further discussed in Section V before conclusions are drawn in Section VI.

II. Related Work

A variety of different wheel-wheg designs have been proposed which change form between a regular circle and a different shape for obstacle traversal. These can be broadly categorized by type of mechanism or deformation type, active or passive activation, and whether the design is bidirectional. A summary of existing designs is presented in Table I. Out of all passive designs, the vast majority fall into the "Pivot Claw" category. These are generally driven by a gear train that rotates claws when the wheel is stalled relative to the shaft.

Our design lies between the "Linkage Claw" and "Passive Pad Deform" categories, and uses the pad deformation to actuate the claw. This design is unique in the passive category for a number of reasons: it does not require a wheel stall to activate (meaning that it will not transform during acceleration or deceleration), it can be made truly bidirectional so that it can traverse and climb obstacles regardless of driving direction, and it can be produced as a single part.

III. Methodology

The overarching ambition of the passively transformable wheel design is to generate a useful passive morphological response driven purely by the geometry of a stepped obstacle on the terrain. The direct advantage of such a solution is

TABLE I
Existing Types of Transformable Wheels

Mechanism	Graphic	Active	Passive
4-Bar Wheel Split	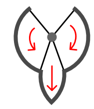	[5], [6], [7]	
Passive Offset Adjustment	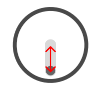		[8]
Independent Leg	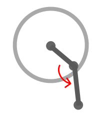	[9]	
Full Robot Split	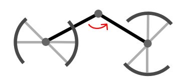	[10], [11]	
Linear Claw	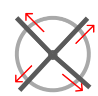	[12], [13]	
Linkage Claw	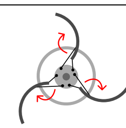	[14], [15], [16], [17]	[18]
Pivot Claw	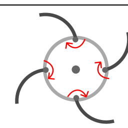	[19], [20], [21]	[22], [23], [24], [25], [26]
Passive Pad Deform	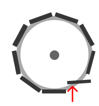		[27], [28]
Origami Expand	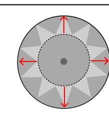	[29]	[30]
Rotary Slip	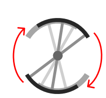		[31]
Tread Split and Rotate	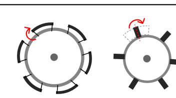	[32], [33]	
Wheel Split	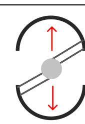	[34], [35]	
Wheel Fold	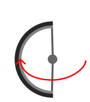	[36]	

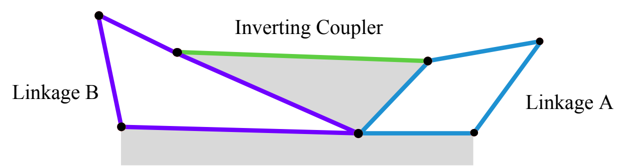

(a)

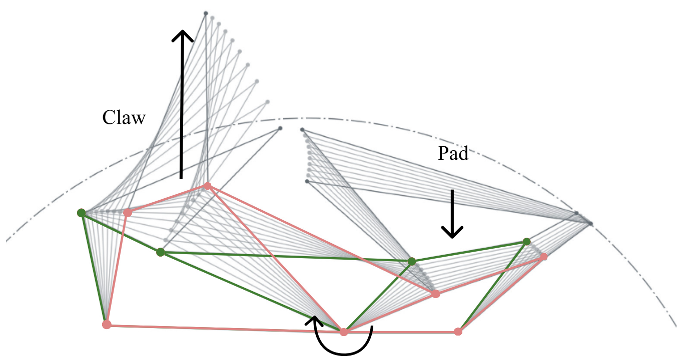

(b)

Fig. 2. Construction and deformation of the motion reversing linkage. (a) Linkage A (the "pad") and Linkage B (the "claw") are joined together by an inverting coupler. (b) When pressed by an obstacle, the pad moves inwards and the claw moves outwards to latch onto the object.

the higher bandwidth of response compared to an actuated solution.

A. Linkage Design

The enabling feature behind our design is a motion reversing linkage, depicted in Fig. 2a. This linkage consists of three sub-parts; two four-bar linkages (Linkage A referred to as the "pad", and Linkage B referred to as the "claw") joined by a coupler that acts like a lever about the central pivot, inverting the motion from the pad. When an obstacle presses against the pad, the claw extends outwards and grips onto the obstacle, shown in Fig. 2b. When it has caught the edge of the object, any downwards force applied by the wheel pushes it further out over the obstacle and provides additional grip.

B. Linkage Kinematics

In this section, we present the kinematic relationship between the pad height p_y and the claw height c_y. As the analytic inverse kinematics of closed chains are often intractable, we parameterize the relationship using the coupler angle θ_{a1}, work forward to each side, and then perform a Taylor approximation which is simpler to invert. The link lengths and vertex labels are shown in Fig. 3.

The fourth order series expansion of the relationship between c_y and θ_{a1} centered around 0.7 radians is

$$c_y \approx c_1 - c_2\theta_{a1} - c_3 c_\theta^2 - c_4 c_\theta^3 - c_5 c_\theta^4 \tag{1}$$

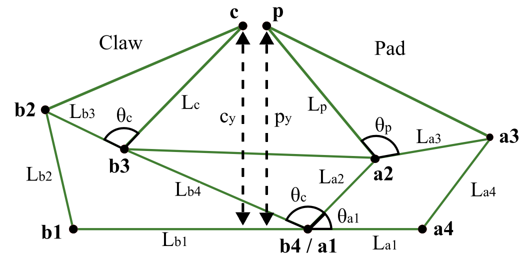

Fig. 3. Linkage diagram with lengths and angles required to calculate the kinematics.

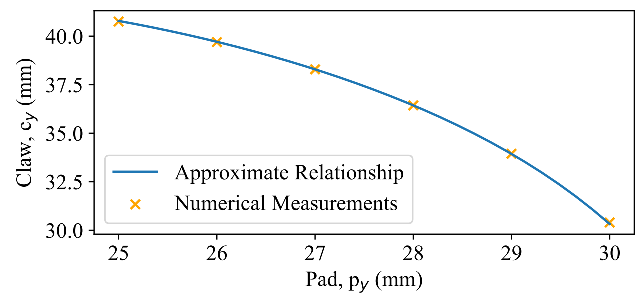

Fig. 4. Kinematic relationship between the displacement of the linkages.

where $c_\theta = \theta_{a1} - 0.7$, $c_1 \approx 59.46$ mm, $c_2 \approx 32.88$ mm, $c_3 \approx 48.26$ mm, $c_4 \approx 55.38$ mm, and $c_5 \approx 161.67$ mm. This approximation has an error of less than 0.2 % over the coupler angle range of $30° - 50°$.

The third order series expansion of the relationship between θ_{a_1} and p_y is

$$p_y \approx p_1 + p_2\theta_{a1} - p_3 p_\theta^2 \tag{2}$$

where $p_\theta = \theta_{a1} - 0.7$, $p_1 \approx 17.18$ mm, $p_2 \approx 15.46$ mm, and $p_3 \approx 12.35$ mm. This approximation has an error of less than 0.3 % over the coupler angle range of $30° - 50°$.

Solving (2) in terms of θ_{a1} and substituting into (1), an approximation for the kinematic relationship between the pad deformation and the claw extension can be obtained as

$$c_y \approx -c_{p1} + c_{p2}p_y - c_{p3}p_y^2 + c_{p4}p_{rt} - c_{p5}p_y p_{rt} \tag{3}$$

where $c_{p1} \approx -2599.15$ mm, $c_{p2} \approx 112.71$ mm, $c_{p3} \approx 2.12$ mm, $c_{p4} \approx 2511.31$ mm, and $c_{p5} \approx 60.75$ mm, and $p_{rt} \approx \sqrt{1 - 0.0305 p_y}$.

This approximation is within 0.3 % over the linkage range when measured against several points on the CAD model. A plot of the input-output relationship is presented in Fig. 4.

C. Flexure Design

To reduce the design to a single part, the six-link mechanism was converted into a flexure that could be manufactured using thermoplastic polyurethane (TPU). The middle of the structure was cut to make the flexure elements thinner, allowing for

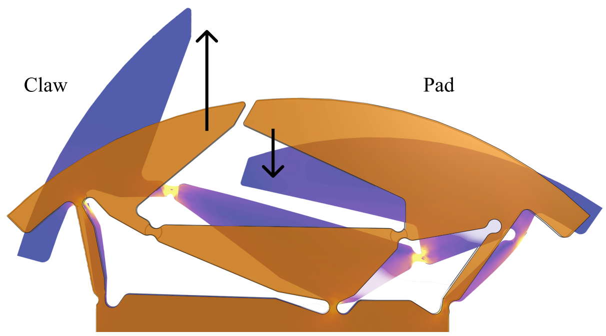

Fig. 5. An individual flexure section and linkage comparison. The flexure can move passively between its natural wheel state (colored in orange in the foreground) and its wheg state with pad pressed and claw extended (colored in purple in the background).

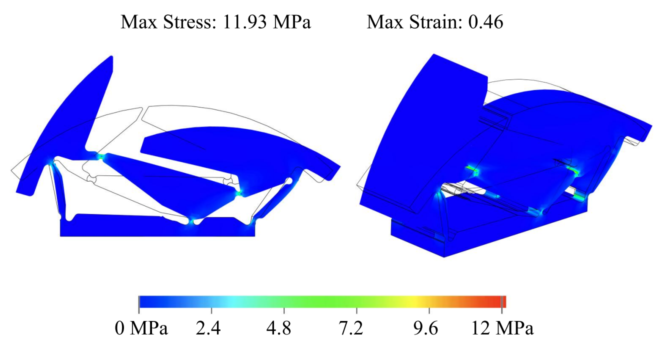

Fig. 6. Results of a linear static FEA analysis, assuming a 26 MPa tensile modulus.

more straightforward tuning of linkage stiffness. The individual flexure segment is presented in Fig. 5. In addition to greater robustness, the flexure provides a restoring force to the natural wheel shape when an obstacle is not present.

TPU with 95 Shore A hardness was chosen to produce the flexure. TPU is the most common flexible 3D printing filament, cost effective, and exhibits characteristics of both plastics and rubbers. It experiences cyclic softening, meaning it does not harden under strain and is well-suited for situations where high count cyclic loading is expected. Due to hysteresis and time dependent effects, TPU acts as if it has short-term memory of its deformation, which allows the wheels to actuate more efficiently during repeated step climbing. From Finite Element Analysis (FEA) simulation, the maximum stress and strain of our design under deflection is 11.9 MPa and 0.46, respectively. In the curve of stress–number of cycles (S-N curve) of TPU fatigue, this equates to $\approx 4 \times 10^6$ cycles [37]. The stress plot from this simulation is shown in Fig. 6.

D. Wheel Design

Multiple flexures are repeated in patterns to form the wheel. We modelled the wheel to have flexures in alternating directions so that it exhibits the same functionality when driven

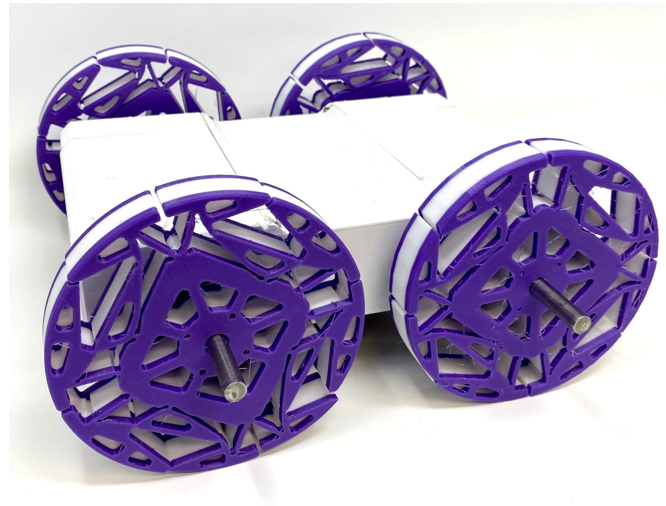

Fig. 7. The four-wheeled mobile robot used to test the performance of different types of wheels. Separate drives allow for independent driving of each wheel.

forwards or backwards. Our design is modular, so that the size, direction, and number of flexures can be adjusted depending on wheel scale, required ride smoothness, and obstacle profiles.

For our design requirements involving wheel size (with a diameter of 120 mm, determined by our robot size), we chose to include four flexures in alternating directions on the PaTS-Wheel. This decision was made based on a trade-off between maximum obstacle height, claw reach, and difficulty of linkage packaging and manufacturing. While a design with only two linkages theoretically achieves the largest claw/pad size (and thus climb height), fitting them without mechanical interference presents design challenges, which could be interesting to explore in future work. Having two linkages would also require as much as an entire wheel rotation before the appropriate linkage would activate and engage with the obstacle. Increasing beyond four linkages could result in a smoother ride and more claws to catch on obstacle edges, but also reduces climbing performance and requires each section to become significantly smaller, causing manufacturing challenges at this scale.

E. Test Robot Design

To test the wheel performance, we designed and built a four-wheeled mobile robot, shown in Fig. 7. Our robot consists of four drive sections allowing for independent drive of each wheel. Since a flexure activates on pressure (and might need to be rotated relative to the obstacle before activating), it is beneficial to allow the front and back axles to spin independently of one another. This lets the back wheels provide forward force and the front wheels rotate until a claw has caught on an obstacle. To keep the supply voltage constant throughout the experiment trials, an external variable voltage supply was used, regulating to 12 V. A 300 g steel mass was placed in the robot cavity to simulate a battery.

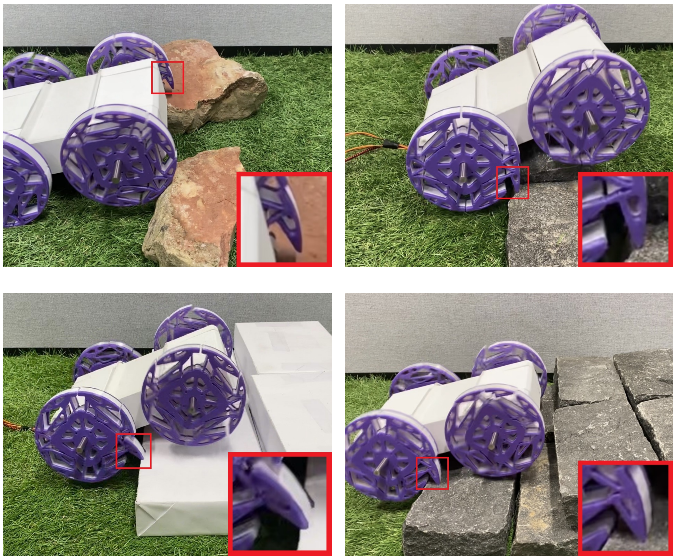

Fig. 8. Examples of the various types of obstacles on which the PaTS-Wheel was tested (clockwise from top-left: rocks, stone blocks, steps of stones, steps of boxes). The amount of wheel deformation, shown inset in the bottom right of each subfigure, depends on the properties of the obstacle and how the wheel interacts with it.

IV. Experiments and Results

We used the mobile robot to test our wheel design on several different obstacles with various physical properties. These included harder objects such as stone blocks and rocks and softer objects like towels and duvets. We also tested the PaTS-Wheel at being able to navigate stairs or steps of boxes and stones. Examples of the robot traversing different types of obstacles are shown in Fig. 8. The amount of wheel deformation depends on the properties of the obstacle. Also, since only the activation of a single linkage is needed for the robot to traverse the obstacle, the orientation of the wheels with respect to each other does not matter.

We designed and produced equivalent wheels and whegs, shown in Fig. 9, to act as a control group for the performance evaluation of our wheel design. These were designed to have the same radius, width, and material layout. The outer surface features were also kept the same where possible. The wheg design was chosen to compromise climbing ability and energy-efficiency-resulting “feet” measuring approximately one-eighth of the circumference. The weight difference between the different wheel types is negligible.

We performed a number of experiments to compare and evaluate the different wheel types: driving power efficiency, vibrational profile, maximum climbing height, and step traversal energy consumption.

Due to ground clearance on the test robot design, our wheels can climb up an obstacle that the full robot is not able to fully traverse. Therefore, the obstacle height results have been split into climbing and traversal: a climb is considered to be lifting the front wheel set above the obstacle, and a traversal is deemed to be lifting the full robot body up and over the obstacle.

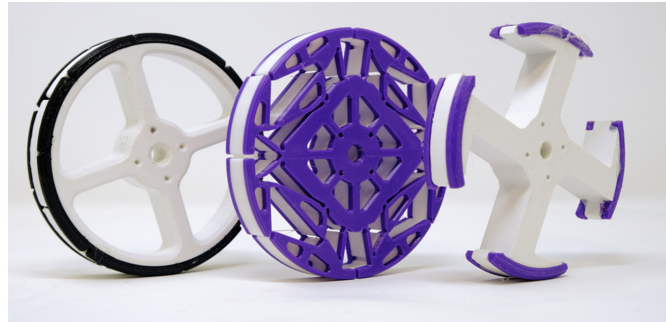

Fig. 9. A comparison between the different wheel types tested. The circular wheel is on the left, the wheg is on the right, and our PaTS-Wheel is in the centre.

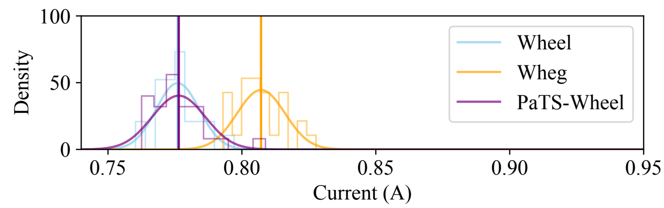

(a)

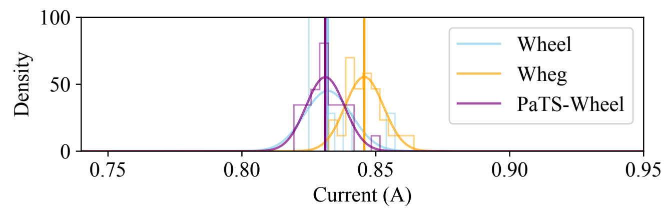

(b)

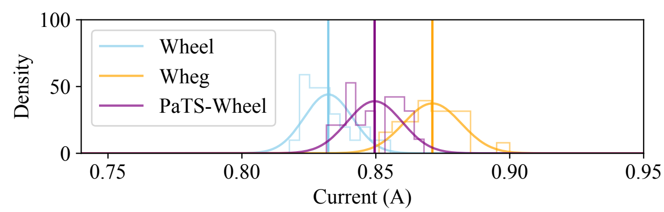

(c)

Fig. 10. Current draw distributions of the various wheel types for the different terrains: (a) wood, (b) artificial grass on wood, and (c) artificial grass on foam.

A. Driving Power Efficiency

We tested the efficiency of robot driving with each of the three wheel types across three physically different surfaces: wooden floor, artificial grass on top of the wooden floor, and artificial grass on top of upholstery foam with thickness of $2''$ (approx. 5 cm). The robot was driven forward for 25 trials over a distance of 1 m and the instantaneous current draw was measured at 100 Hz using an ACS712 Hall Effect Current Sensor connected to a Raspberry Pi Pico. The current draw distributions for the different terrains are plotted in Fig. 10.

On both of the rigid surfaces (wood in Fig. 10a and artificial grass in Fig. 10b), there was no significant difference between the power consumption of the “pure” wheel and the PaTS-Wheel. It is interesting to note that the hybrid solution moves

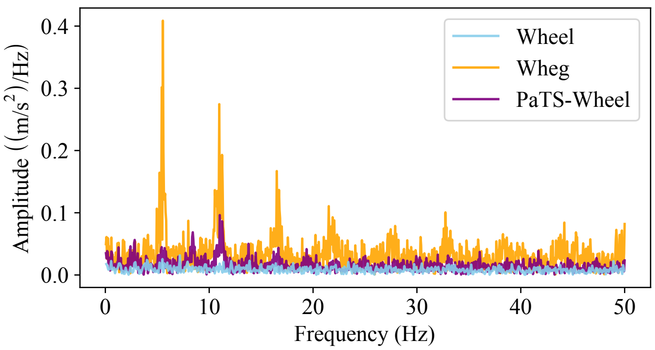

Fig. 11. Fourier series of the linear acceleration for the three modes of locomotion.

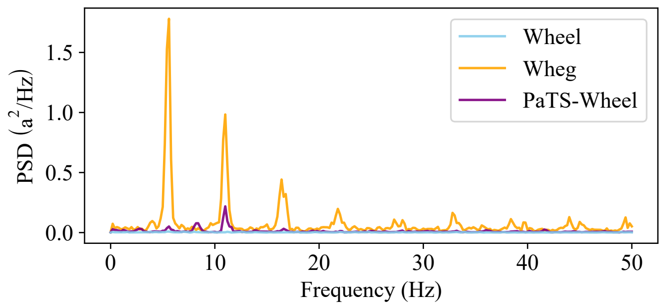

Fig. 12. Power spectral density (PSD) plot of linear acceleration magnitude.

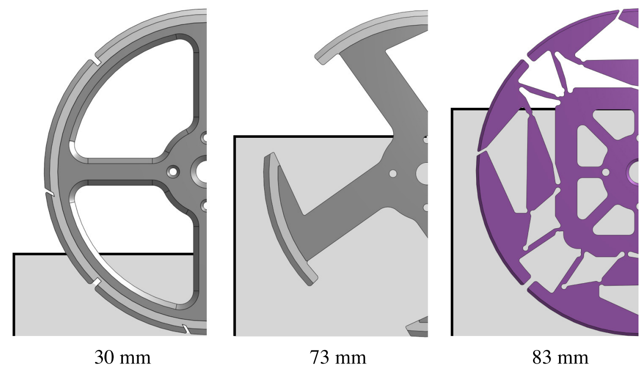

Fig. 13. Maximum climb height achieved with a 100% success rate on each wheel, relative to their common size. The wheel can traverse obstacles with heights approx. 25 % its diameter, the wheg can traverse approx. 61 % its diameter, and the PaTS-Wheel can traverse approx. 70 % its diameter.

to a form between a wheel and a wheg on spongy ground (Fig. 10c). This is due to the compliance of the artificial grass and foam making the linkage flex, resulting in higher grip on the soft terrain. Our solution is between $1.7 - 3.8$ % more power efficient than the wheg which excessively grips the foam.

B. Vibrational Profile

In order to measure the vibrational profiles of the three wheel types, an LSM6DSOX 6-DoF IMU (Adafruit Industries) was placed in the middle of the vehicle. The robot was driven forward at a constant velocity and both linear acceleration and angular velocity were recorded. Fourier transforms were performed on the recorded linear acceleration and angular velocity of each wheel type, and are presented in Fig. 11.

It can be seen that whegs exhibit the highest amplitude of acceleration transition frequency components followed by the PaTS-Wheel and regular wheels. The root mean square (RMS) acceleration of the PaTS-Wheel is approximately 25 % that of the wheg. In the case of whegs, the spikes in the frequency domain appear first around 6 Hz—four times the frequency of the shaft—and repeat periodically. The PaTS-Wheel has a spike around eight times the frequency of the shaft, as there are eight semi-independent segments. This indicates that while our design incorporates useful morphological features for hooking onto obstacles to surmount them, similar to whegs, it does not demonstrate the same level of impulsive contact forces.

Examining the vibrational power density yields similar observations. A power spectral density (PSD) plot using Welch's method is presented in Fig. 12, and shows that the cumulative vibrational energy of the PaTS-Wheel is approx. 37 % that of the wheg.

C. Maximum Climbing Height

The maximum climbing height is considered to be the highest step obstacle over which a wheel candidate can reliably lift and pull its front axle. Each wheel type was tested in 5 trials at lifting itself up within a time limit of 5 seconds. On higher obstacles we noticed that our design could take a few seconds to activate, and it will be interesting to attempt marginal time improvements in future work. A design was considered reliable if it climbed the obstacle successfully over all 5 trials within the time limit.

Different obstacle heights were tested in 10 mm increments, and maximum results relative to wheel types are visualized in Fig. 13. The PaTS-Wheel design not only matched, but even outperformed the reference wheg design, proving that we have met our obstacle climb design requirement.

Fig. 14 shows the progression of our wheel coming into contact with and traversing an obstacle. The claw extends and grips the object when the pad is pressed, allowing the wheel to latch on and pull itself upwards. The wheel resumes its natural shape as the robot traverses the obstacle.

D. Step Traversal Energy Consumption

To measure the full energy consumption of the robot traversing a step obstacle, the robot was driven forward 70 cm with a 17 mm width step in the middle. Cumulative energy consumption was measured for the robot to complete its course traversing the obstacle. A series of 5 trials was performed for each wheel while increasing the obstacle height by 10 mm until the wheel failed to traverse. The results from these experiments are presented in Fig. 15.

As can be seen, the pure wheel and PaTS-Wheel energy consumption match closely for lower obstacles. At obstacle heights around $20 - 30$ mm ($\approx 16 - 25$ % of the wheel diameter) there is a transition in both the wheel and PaTS-Wheel, denoted by the increase in energy consumption. This

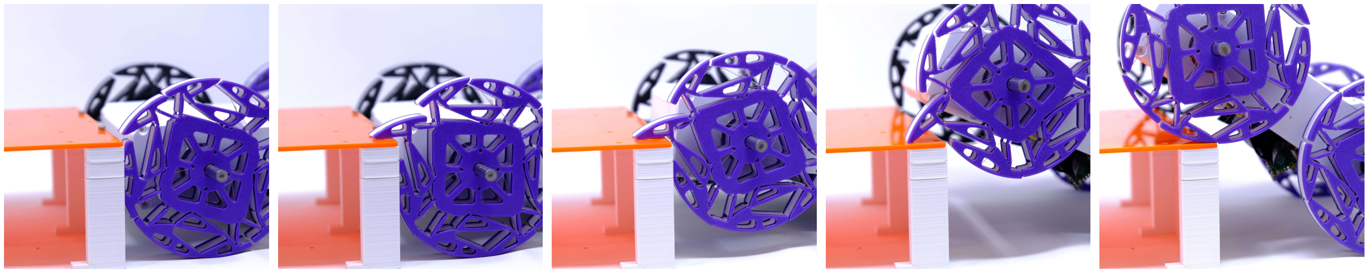

Fig. 14. Progression of the PaTS-Wheel structure as the robot comes into contact with and traverses an obstacle. Note how when the pad is pressed, the claw extends and latches onto the obstacle. The wheel uses the forward drive of the robot to push itself onto the obstacle at which time it resumes its natural shape for more efficient and smoother locomotion.

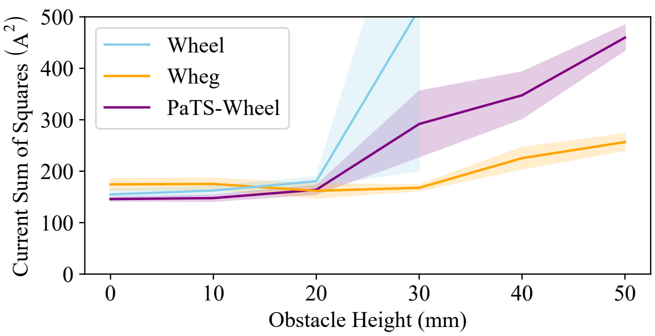

Fig. 15. Cumulative energy required to traverse obstacles of various heights. The shaded regions show the standard deviation in each case.

marks the failure point of the wheel, and where our design begins to transform itself to lift itself over the obstacle. Interestingly, the energy consumption of the wheg appears to decrease around this point. One potential explanation is that the obstacle profile allows the wheg to launch itself over the obstacle and reach the finish line quicker, thus reducing overall energy consumption. This presents an interesting efficiency target for future design work.

V. Discussion

The key novelties of the suggested robot locomotion solution lie in its single-part and bidirectional design, capable of transforming passively from a regular wheel to one equipped with hooks, in response to the terrain's geometric features.

From wheels to articulated legs, different designs of robot locomotion try to determine the best contact dynamics with the most frequently found features on the ground. While wheels have been proven to be efficient and stable on relatively flat grounds, articulated legs have the advantage of "sampling" the terrain to the robot's advantage. However, they lead to kinematic and dynamic challenges for real-time control. Whegs with fixed spacing between non-articulated legs in a rimless wheel arrangement have been a popular compromise. Whegs also lead to punctuated transitions in acceleration on terrains where the advantage of legs is not apparent. In this paper, we present a new metamorphic wheel that self-transforms to a wheg when required by the terrain and returns back to a wheel morphology on flat ground. The capability of our new design to allow the terrain's geometric features to influence its morphological state has resulted in increased locomotion efficiency, with fewer spikes in the acceleration profile. Moreover, it enables traversal over obstacles that equivalent whegs and wheels could not match.

The aforementioned efficiency gains and bidirectional operation ability without requiring active control systems could lead to broader applications and enhance the functionality of robots and vehicles, particularly in unstructured, cluttered, or otherwise challenging environments. Some examples of these include disaster response, agricultural settings, and environmental monitoring.

VI. Conclusions

In this paper, we presented the PaTS-Wheel, a Passively-Transformable Single-part Wheel for obstacle traversal and navigation in unstructured environments. The design methodology and implementation were detailed, and results presented from a series of real world tests. Our hybrid wheel requires no additional actuators or bespoke control schemes and is inherently robust due to its single-part construction. We tested the performance of the PaTS-Wheel in comparison to a pure wheel and a traditional wheg across a number of experiments where all three models have the same diameter of $120\ \mathrm{mm}$. Our novel design outperforms the wheg and matches the pure wheel in terms of energy efficiency. It also achieves superior height climbing ability, recording $100\ \%$ success rate traversing obstacles with a height of $83\ \mathrm{mm}$ ($\approx 70\ \%$ its diameter), higher than the results obtained for an equivalent wheel at $30\ \mathrm{mm}$ ($\approx 25\ \%$ its diameter) and an equivalent wheg at $73\ \mathrm{mm}$ ($\approx 61\ \%$ its diameter). Additionally, in comparison to the wheg, less vibrations are experienced, likely improving the longevity of a robot/vehicle and its payload as well as the accuracy of onboard sensors. Our results suggest that this new design combines the benefits of wheels and whegs and could be added to mobile robots to improve capability and efficiency of locomotion and traversal across unstructured and cluttered environments.

References

[1] R. D. Quinn, J. T. Offi, D. A. Kingsley, and R. E. Ritzmann, "Improved mobility through abstracted biological principles," in *IEEE/RSJ International Conference on Intelligent Robots and Systems*, vol. 3. IEEE, 2002, pp. 2652–2657.

[2] R. T. Schroer, M. J. Boggess, R. J. Bachmann, R. D. Quinn, and R. E. Ritzmann, "Comparing cockroach and whegs robot body motions," in *IEEE International Conference on Robotics and Automation, 2004. Proceedings. ICRA'04. 2004*, vol. 4. IEEE, 2004, pp. 3288–3293.

[3] U. Saranli, M. Buehler, and D. E. Koditschek, "RHex: A simple and highly mobile hexapod robot," *The International Journal of Robotics Research*, vol. 20, no. 7, pp. 616–631, 2001.

[4] B. W. Mulvey, T. D. Lalitharatne, and T. Nanayakkara, "DeforMoBot: A bio-inspired deformable mobile robot for navigation among obstacles," *IEEE Robotics and Automation Letters*, vol. 8, no. 6, pp. 3828–3835, 2023.

[5] H.-Y. Chen, T.-H. Wang, K.-C. Ho, C.-Y. Ko, P.-C. Lin, and P.-C. Lin, "Development of a novel leg-wheel module with fast transformation and leaping capability," *Mechanism and Machine Theory*, vol. 163, p. 104348, 2021.

[6] Y. Xue, X. Yuan, Y. Wang, Y. Yang, S. Lu, B. Zhang, J. Lai, J. Wang, and X. Xiao, "Lywal: a leg-wheel transformable quadruped robot with picking up and transport functions," in *2021 IEEE International Conference on Robotics and Automation (ICRA)*. IEEE, 2021, pp. 2935–2941.

[7] A. Yeldan, A. Arora, and G. S. Soh, "QuadRunner: A transformable quasi-wheel quadruped," in *2022 International Conference on Robotics and Automation (ICRA)*. IEEE, 2022, pp. 4694–4700.

[8] K. Hodo and Y. Yamada, "Passive offset adjusting wheel mechanism," in *2022 IEEE/ASME International Conference on Advanced Intelligent Mechatronics (AIM)*. IEEE, 2022, pp. 769–774.

[9] Z. Wei, G. Song, Y. Zhang, H. Sun, and G. Qiao, "Transleg: A wire-driven leg-wheel robot with a compliant spine," in *2016 IEEE international Conference on Information and Automation (ICIA)*. IEEE, 2016, pp. 7–12.

[10] J.-J. Chou and L.-S. Yang, "Innovative design of a claw-wheel transformable robot," in *2013 IEEE International Conference on Robotics and Automation*. IEEE, 2013, pp. 1337–1342.

[11] L.-H. Pan, C.-N. Kuo, C.-Y. Huang, and J. J. Chou, "The claw-wheel transformable hybrid robot with reliable stair climbing and high maneuverability," in *2016 IEEE International Conference on Automation Science and Engineering (CASE)*. IEEE, 2016, pp. 233–238.

[12] N. Moriya, H. Shigemune, and H. Sawada, "A robotic wheel locally transforming the diameter for the locomotion on rough terrain," in *2020 IEEE International Conference on Mechatronics and Automation (ICMA)*. IEEE, 2020, pp. 1257–1262.

[13] S.-S. Yun, J.-Y. Lee, G.-P. Jung, and K.-J. Cho, "Development of a transformable wheel actuated by soft pneumatic actuators," *International Journal of Control, Automation and Systems*, vol. 15, pp. 36–44, 2017.

[14] Y. Lee, S. Ryu, J. H. Won, S. Kim, H. S. Kim, and T. Seo, "Modular two-degree-of-freedom transformable wheels capable of overcoming obstacle," *IEEE Robotics and Automation Letters*, vol. 7, no. 2, pp. 914–920, 2021.

[15] Q. Xu, H. Xu, K. Xiong, Q. Zhou, and W. Guo, "Design and analysis of a bi-directional transformable wheel robot trimode," in *2021 IEEE/RSJ International Conference on Intelligent Robots and Systems (IROS)*. IEEE, 2021, pp. 8396–8403.

[16] Y. Kim, Y. Lee, S. Lee, J. Kim, H. S. Kim, and T. Seo, "STEP: A new mobile platform with 2-DOF transformable wheels for service robots," *IEEE/ASME Transactions on Mechatronics*, vol. 25, no. 4, pp. 1859–1868, 2020.

[17] X. Zhao, W. Su, and S. Zhang, "The simulation and analysis of a new rescue robot with transformable wheels," in *2019 2nd World Conference on Mechanical Engineering and Intelligent Manufacturing (WCMEIM)*. IEEE, 2019, pp. 545–548.

[18] L. Bai, J. Guan, X. Chen, J. Hou, and W. Duan, "An optional passive/active transformable wheel-legged mobility concept for search and rescue robots," *Robotics and Autonomous Systems*, vol. 107, pp. 145–155, 2018.

[19] A. K. Tanyıldızı, "Design, control and stabilization of a transformable wheeled fire fighting robot with a fire-extinguishing, ball-shooting turret," *Machines*, vol. 11, no. 4, p. 492, 2023.

[20] Z. Lv and B. Yuan, "Design and analysis of transformable wheel-legged mobile robot," *Academic Journal of Science and Technology*, vol. 4, no. 2, pp. 83–87, 2022.

[21] İ. Mertyüz, A. K. Tanyıldızı, B. Taşar, A. B. Tatar, and O. Yakut, "FUHAR: A transformable wheel-legged hybrid mobile robot," *Robotics and Autonomous Systems*, vol. 133, p. 103627, 2020.

[22] R. Woolley, J. Timmis, and A. M. Tyrrell, "Cylindabot: transformable wheg robot traversing stepped and sloped environments," *Robotics*, vol. 10, no. 3, p. 104, 2021.

[23] Y. Tao, C. Gao, Y. Shi, M. Li, M. Zhang, and D. Liu, "Analysis of motion characteristics and stability of mobile robot based on a transformable wheel mechanism," *Applied Sciences*, vol. 12, no. 23, p. 12348, 2022.

[24] Y. Shi, M. Zhang, M. Li, and X. Zhang, "Design and analysis of a wheel-leg hybrid robot with passive transformable wheels," *Symmetry*, vol. 15, no. 4, p. 800, 2023.

[25] Y.-S. Kim, G.-P. Jung, H. Kim, K.-J. Cho, and C.-N. Chu, "Wheel transformer: A miniaturized terrain adaptive robot with passively transformed wheels," in *2013 IEEE International Conference on Robotics and Automation*. IEEE, 2013, pp. 5625–5630.

[26] C. Zheng and K. Lee, "WheeLeR: Wheel-leg reconfigurable mechanism with passive gears for mobile robot applications," in *2019 International Conference on Robotics and Automation (ICRA)*. IEEE, 2019, pp. 9292–9298.

[27] Y. Chen, A. Kamioka, M. Iwase, J. Inoue, and Y. Satoh, "Design and analysis of transformable wheel with pivoting-head mechanism," *Applied Mechanics*, vol. 4, no. 1, pp. 70–89, 2023.

[28] K. A. Daltorio, T. E. Wei, S. N. Gorb, R. E. Ritzmann, and R. D. Quinn, "Passive foot design and contact area analysis for climbing mini-whegs," in *Proceedings 2007 IEEE International Conference on Robotics and Automation*. IEEE, 2007, pp. 1274–1279.

[29] L. M. Fonseca and M. A. Savi, "Nonlinear dynamics of an autonomous robot with deformable origami wheels," *International Journal of Non-Linear Mechanics*, vol. 125, p. 103533, 2020.

[30] D.-Y. Lee, G.-P. Jung, M.-K. Sin, S.-H. Ahn, and K.-J. Cho, "Deformable wheel robot based on origami structure," in *2013 IEEE International Conference on Robotics and Automation*. IEEE, 2013, pp. 5612–5617.

[31] A. Vijaychandra, C. Alex, M. Mathews, and A. A. Sathar, "Amphibious wheels with a passive slip mechanism for transformation," in *2019 IEEE 4th International Conference on Advanced Robotics and Mechatronics (ICARM)*. IEEE, 2019, pp. 960–965.

[32] X. Xie, F. Gao, C. Huang, and W. Zeng, "Design and development of a new transformable wheel used in amphibious all-terrain vehicles (A-ATV)," *Journal of Terramechanics*, vol. 69, pp. 45–61, 2017.

[33] Y. She, C. J. Hurd, and H.-J. Su, "A transformable wheel robot with a passive leg," in *2015 IEEE/RSJ International Conference on Intelligent Robots and Systems (IROS)*. IEEE, 2015, pp. 4165–4170.

[34] T. Ma, H. Cheng, Z. Cheng, C. Wang, M. Duan, N. Jiang, H. Wang, and S. Yao, "R-Taichi: A quadruped robot with deformed wheels," in *2023 IEEE International Conference on Mechatronics and Automation (ICMA)*. IEEE, 2023, pp. 1221–1226.

[35] C. Dai, X. Liu, J. Zhou, Z. Liu, Z. Zhu, and Z. Jia, "SWhegPro: A novel robust wheel-leg transformable robot," in *2022 IEEE International Conference on Robotics and Biomimetics (ROBIO)*. IEEE, 2022, pp. 421–426.

[36] S.-C. Chen, K.-J. Huang, W.-H. Chen, S.-Y. Shen, C.-H. Li, and P.-C. Lin, "Quattroped: a leg–wheel transformable robot," *IEEE/ASME Transactions on Mechatronics*, vol. 19, no. 2, pp. 730–742, 2013.

[37] S. Wang, S. Tang, C. He, and Q. Wang, "Cyclic deformation and fatigue failure mechanisms of thermoplastic polyurethane in high cycle fatigue," *Polymers*, vol. 15, no. 4, p. 899, 2023.